

A candidate for central tidal disruption event in the broad line AGN SDSS J1605 with double-peaked broad H β

Xue-Guang Zhang^{*}

Guangxi Key Laboratory for Relativistic Astrophysics, School of Physical Science and Technology, Guangxi University, Nanning, 530004, P. R. China

8 February 2024

ABSTRACT

In this letter, motivated by double-peaked broad Balmer emission lines probably related to tidal disruption events (TDEs), a potential TDE candidate is reported in SDSS J160536+134838 (=SDSS J1605) at $z \sim 0.44$ having quasar-like spectrum but with double-peaked broad H β . The long-term CSS light curve can be naturally described by a main-sequence star of $2.82^{+0.20}_{-0.19} M_{\odot}$ disrupted by the central black hole (BH) of $144^{+26}_{-21} \times 10^6 M_{\odot}$ in SDSS J1605. Meanwhile, the ASAS-SN light curves afterwards show none apparent trend variability, indicating the bright CSS flare in SDSS J1605 unique and different enough from variability of normal AGN. Furthermore, there is a consistency between the TDE model determined sizes of debris with the sizes of emission regions for the double-peaked broad H β described by the accretion disk model, supporting the disk-like BLRs probably related to a central TDE in SDSS J1605. And the virial BH mass ~ 7 times higher than the TDE model determined value can be naturally explained by R-L relation determined BLRs sizes very larger than the actual distance of emission regions related to TDEs debris in SDSS J1605. Although no clear conclusion on double-peaked broad lines absolutely related to TDEs, the results here provide clues to detect potential TDEs in AGN with double-peaked broad lines.

Key words: galaxies:active - galaxies:nuclei - quasars:emission lines - transients:tidal disruption event

1 INTRODUCTION

Tidal Disruption Events (TDEs) have been studied for more than four decades (Rees 1988; Loeb & Ulmer 1997; Gezari et al. 2006; Guillochon & Ramirez-Ruiz 2013; Guillochon et al. 2014; Wang et al. 2018; Mockler et al. 2019; Thorp et al. 2019; Ryu et al. 2020; Lynch & Ogilvie 2021; Zhou et al. 2021), with accreting fallback debris from stars tidally disrupted by central supermassive black holes (SMBHs) leading to apparent time-dependent variability. More recent review on theoretical TDEs can be found in Stone et al. (2019). TDEs are commonly accepted as the better indicators to SMBHs and BH accreting systems, more and more TDEs have been detected and reported in the literature (see <https://tde.space/>), especially through current public sky survey projects.

Descriptions of one to two known TDEs candidates from each current survey are given as follows. Through the SDSS Stripe82 database, Velzen et al. (2011) have reported two TDEs candidates in SDSS non-active galaxies. Through the Catalina Sky Survey (CSS), Drake et al. (2011) have reported a probable TDE candidate in narrow-line Seyfert 1 galaxy CSS100217. Through the project of Panoramic Survey Telescope And Rapid Response System (Pan-STARRS), Gezari et al. (2012); Chornock et al. (2014) have reported robust TDEs candidates of PS1-10jh and PS1-11af in inactive galaxies, due to their ultraviolet-optical flares well described by the theoretical TDE model. Through the project of Palomar Transient Factory (PTF), Blagorodnova et al. (2017); van Velzen et al. (2019) have reported two TDEs candidates of iPTF16fnl and AT2018zr/PS18kh.

Through the project of Optical Gravitational Lensing Experiment (OGLE), Wyrzykowski et al. (2017); Gromadzki et al. (2019) have reported TDE candidates of OGLE16aaa and OGLE17aaj. Through the project of All-Sky Automated Survey for SuperNovae (ASAS-SN), Holoien et al. (2014, 2016); Hinkle et al. (2021) have reported the known TDEs candidates of ASASSN-14ae, ASASSN-14li and ASASSN-19dj. Through the Caltech-NRAO Stripe82 Survey (CNSS), Anderson et al. (2020) have reported the TDE candidate of CNSS J0019+00. Through the project of Zwicky Transient Facility (ZTF), Lee et al. (2020); Stein et al. (2021) have reported the TDE candidate of AT2019DSG. Through the project of the Global astrometric interferometer for astrophysics (Gaia), Kostrzewa-Rutkowska et al. (2018) have listed a small sample of TDEs candidates among the nuclear transients reported by the Gaia Science Alerts team. Through the project of the Asteroid Terrestrial Impact Last Alert System (ATLAS), Hinkle et al. (2023a) have discovered the TDE candidate ATLAS18mlw, a faint and fast TDE in a quiescent galaxy. More recently, two large samples of dozens of new TDE candidates can be found in van Velzen et al. (2021) from the First Half of ZTF Survey observations along with Swift UV and X-ray follow-up observations and in Sazonov et al. (2021) from the SRG all-sky survey observations and then confirmed by optical follow-up observations. More recent review on observational properties of the reported TDEs can be found in Gezari (2021).

Among the reported TDEs candidates, it can be commonly accepted that weak narrow emission lines (especially weak [O III] λ 5007Å emission lines) but broad Balmer and He II emission lines are in their optical spectra. In part of TDEs candidates, the reported broad emission lines could be related to disk-like struc-

^{*} Corresponding author Email: xgzhang@gxu.edu.cn

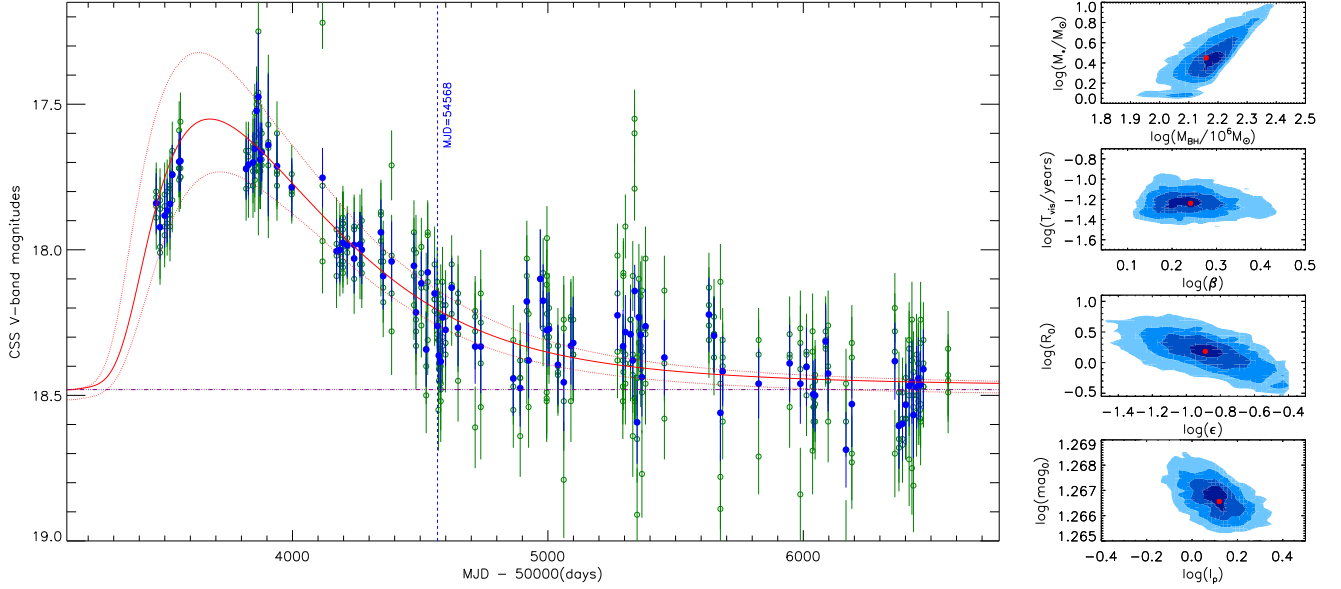


Figure 1. Left panel shows the best descriptions (solid red line) to the CSS V-band light curve (open circles plus error bars in dark green) by the theoretical TDE model expected variability plus a non-variability component. Solid circles plus error bars in blue show the corresponding 5days binned light curve. Dashed red lines show the confidence bands to the best descriptions, after accepted the uncertainties of the TDE model parameters. Horizontal purple line shows the determined non-TDE component with magnitude about 18.48. The vertical dashed blue line marks the position MJD=54568 on which the SDSS spectrum is observed. Right panels show the MCMC determined two-dimensional posterior distributions in contour of the TDE model parameters and mag_0 . In each right panel, the five contour levels show the corresponding 0.1, 0.3, 0.5, 0.7 and 0.9 of the two-dimensional volume contained, and solid red circle marks the positions of the accepted values of the model parameters.

tures from TDE debris, such as SDSS J0159 (Merloni et al. 2015; Zhang 2021), PTF09djl (Liu et al. 2017), PS18kh (Holoien et al. 2019), AT2018hyz (Short et al. 2020; Hung et al. 2020), AT2019qiz (Short et al. 2023), etc., indicating the reported optical broad emission lines in part of TDEs candidates are not related to normal broad emission line regions (BLRs) in broad line AGN (BLAGN) but tightly related to TDE debris. In other words, potential TDEs candidates could be probably detected in BLAGN with double-peaked broad Balmer emission lines (double-peaked BLAGN). Motivated by the point that double-peaked BLAGN could possibly harbor potential TDEs, the SDSS J160536+134838 (=SDSS J1605) at redshift $z \sim 0.44$ is collected as the subject of this letter, not only due to its broad Balmer lines described by a disk-like component but also due to its TDE expected photometric variability. Not similar as the previous reported TDEs in nearby inactive galaxies and/or in weak active galaxies and/or in changing-look AGN, the SDSS J1605 harboring a potential central TDE reported in this letter has not only strong and apparent broad Balmer emission lines but also strong $[O\text{ III}]\lambda 5007\text{\AA}$ emission lines.

This letter is organized as follows. Section 2 presents main results on photometric variability properties, and necessary discussions. Section 3 shows main results on broad emission lines and necessary discussions. Section 4 gives final conclusions. And in the Letter, we have adopted the cosmological parameters of $H_0 = 70\text{km} \cdot \text{s}^{-1}\text{Mpc}^{-1}$, $\Omega_\Lambda = 0.7$ and $\Omega_m = 0.3$.

2 LONG-TERM VARIABILITY IN SDSS J1605

Long-term photometric V-band light curve of SDSS J1605 with $z \sim 0.44$ is collected from CSS (Drake et al. 2009) with MJD from

53466 to 56567 shown in the left panel of Fig. 1. Meanwhile, the corresponding high-quality 5days binned light curve is also shown. There are two points we can find. First, in the 4 years with MJD from ~ 5200 to ~ 6600 , there are not apparent trend variability in SDSS J1605. Second, there is a smooth declining trend with MJD from ~ 3800 to ~ 5000 , similar as the variability pattern expected from a TDE. Here, the trend variability amplitudes are about 0.75mag and 0.02mag simply determined by a linear function applied to the light curve (also the binned light curve) with MJD smaller than 5200 and larger than 5200, respectively. Therefore, we said there are not trend variability in the light curve with MJD larger than 5200.

Now, let's check whether the standard theoretical TDE model can be applied to describe the variability of SDSS J1605. The more recent detailed descriptions on the theoretical TDE model can be found in Guillochon & Ramirez-Ruiz (2013); Guillochon et al. (2014, 2018); Mockler et al. (2019). The corresponding public codes on the theoretical TDE model can be found in TDEFIT (<https://tde.space/tdefit/>) and MOSFIT (<http://mosfit.readthedocs.io/>). Here, based on the more recent discussions in Mockler et al. (2019), and similar as what we have recently done in Zhang (2022a,b,c, 2023a) to model/simulate TDE expected time dependent variability, simple descriptions on applications of standard theoretical TDE model are given as follows by four steps.

First, based on TDEFIT/MOSFIT provided fallback material rates $\dot{M}_{fbt} = dm/de \times de/dt$ for standard cases with a $1M_\odot$ main sequence star tidally disrupted by a central SMBH with mass $M_{BH} = 10^6 M_\odot$, standard templates of viscous-delayed accretion rates \dot{M}_{at} (described in Mockler et al. 2019) can be created by

$$\dot{M}_{at} = \frac{\exp(-t/T_{vis})}{T_{vis}} \int_0^t \exp(t'/T_{vis}) \dot{M}_{fbt} dt' \quad (1)$$

. And a grid of 31 $\log(T_{vis,t}/\text{years})$ range from -3 to 0 are applied to create templates of \dot{M}_{at} for each impact parameter β applied in TDEFIT/MOSFIT, leading to the created templates of \dot{M}_{at} including 736 (640) time-dependent viscous-delayed accretion rates for 31 different T_{vis} of each 23 (20) impact parameters for the main-sequence star with polytropic index γ of 4/3 (5/3).

Second, simple linear interpretations are applied to determine viscous-delayed accretion rate \dot{M}_a with input parameters of β and T_{vis} different from the list values in β_t for the standard cases listed in TDEFIT/MOSFIT and in $T_{vis,t}$ discussed above,

$$\begin{aligned} \dot{M}_a(T_{vis}, \beta_1) &= \dot{M}_{at}(T_{vis1}, \beta_1) + \\ &\frac{T_{vis} - T_{vis1}}{T_{vis2} - T_{vis1}} (\dot{M}_{at}(T_{vis2}, \beta_1) - \dot{M}_{at}(T_{vis1}, \beta_1)) \\ \dot{M}_a(T_{vis}, \beta_2) &= \dot{M}_{at}(T_{vis1}, \beta_2) + \\ &\frac{T_{vis} - T_{vis1}}{T_{vis2} - T_{vis1}} (\dot{M}_{at}(T_{vis2}, \beta_2) - \dot{M}_{at}(T_{vis1}, \beta_2)) \\ \dot{M}_a(T_{vis}, \beta) &= \dot{M}_a(T_{vis}, \beta_1) + \\ &\frac{\beta - \beta_1}{\beta_2 - \beta_1} (\dot{M}_a(T_{vis}, \beta_2) - \dot{M}_a(T_{vis}, \beta_1)) \end{aligned} \quad (2)$$

with β_1, β_2 in the β_t as the two values nearer to the input β , and T_{vis1}, T_{vis2} in the $T_{vis,t}$ as the two values nearer to the input T_{vis} .

Third, for a TDE with input model parameters of M_{BH} and M_* different from $10^6 M_\odot$ and $1 M_\odot$, the actual viscous-delayed accretion rates \dot{M} and the corresponding time information in observer frame are created from the viscous-delayed accretion rates $\dot{M}_a(T_{vis}, \beta)$ by the following scaling relations,

$$\begin{aligned} \dot{M} &= M_{BH,6}^{-0.5} \times M_*^2 \times R_*^{-1.5} \times \dot{M}_a(T_{vis}, \beta) \\ t &= (1+z) \times M_{BH}^{0.5} \times M_*^{-1} \times R_*^{1.5} \times t_a(T_{vis}, \beta) \end{aligned} \quad (3)$$

, where $M_{BH,6}$, M_* , R_* and z represent central BH mass in units of $10^6 M_\odot$, stellar mass in units of M_\odot , stellar radius in units of R_\odot and redshift of host galaxy of a TDE, respectively. And the mass-radius relation in Tout (1996) has been accepted in the Letter for main-sequence stars.

Fourth, the time-dependent output spectrum from the accreting process with the TDE model expected accretion rate $\dot{M}(t)$ can be determined by the simple black-body photosphere model as discussed in Mockler et al. (2019),

$$\begin{aligned} F_\lambda(t) &= \frac{2\pi Gc^2}{\lambda^5} \frac{1}{\exp(hc/(k\lambda T_p(t))) - 1} \left(\frac{R_p(t)}{D}\right)^2 \\ R_p(t) &= R_0 \times a_p \left(\frac{\epsilon \dot{M}(t)c^2}{1.3 \times 10^{38} M_{BH}/M_\odot}\right)^{1/p} \\ T_p(t) &= \left(\frac{\epsilon \dot{M}(t)c^2}{4\pi\sigma_{SB}R_p^2}\right)^{1/4} \quad a_p = (GM_{BH} \times (\frac{t_p}{\pi})^2)^{1/3} \end{aligned} \quad (4)$$

where D means the distance to the earth calculated by redshift z , k is the Boltzmann constant, T_p and R_p represent the time-dependent effective temperature and radius of the photosphere, ϵ is the energy transfer efficiency smaller than 0.4, σ_{SB} is the Stefan-Boltzmann constant, t_p is the time information of the peak accretion rate. Then, time-dependent apparent magnitudes $mag(t)$ can be well determined through transmission curve of the accepted filters convolved with the $F_\lambda(t)$. In this letter, the commonly applied Johnson V filter is accepted.

Therefore, based on the four steps above, apparent magnitudes $mag_m(t)$ can be created by theoretical TDE model with eight parameters (redshift $z = 0.44096$ accepted to SDSS J1605) of central

Table 1. Parameters for the emission line components

model parameters of accretion disk model for broad H β					
$r_0 = 63 \pm 14$, $r_1 = 530 \pm 30$, $\sin(i) = 0.27 \pm 0.01$, $q = 0.67 \pm 0.32$					
$e = 0.22 \pm 0.02$, $\sigma_L = 980 \pm 160\text{km/s}$, $\phi_0 = 15 \pm 2^\circ$					
Gaussian parameters of narrow emission lines around H β					
$\lambda_0(\text{\AA})$	$\sigma(\text{\AA})$	flux	$\lambda_0(\text{\AA})$	$\sigma(\text{\AA})$	flux
4861.5 \pm 0.3	2.8 \pm 0.3	28 \pm 3	4864.4 \pm 0.4	11.4 \pm 0.3	68 \pm 13
5007.2 \pm 0.1	2.8 \pm 0.1	434 \pm 6	5011.5 \pm 0.4	12.5 \pm 0.4	245 \pm 8
4845.5 \pm 2.1	30.9 \pm 2.4	479 \pm 45	4904.3 \pm 2.3	35.6 \pm 3.1	670 \pm 91

Note: The first (last) three columns listed in the last two rows show the central wavelength in units of \AA , the second moment in units of \AA and flux in units of $10^{-17}\text{erg/s/cm}^2$ for the core (extended) components of narrow H β and [O III] λ 5007 \AA , and for the two broad Gaussian components in the broad H β .

BH mass M_{BH} , mass M_* and polytropic index γ (4/3 or 5/3) of the disrupted main-sequence star, the impact parameter β , the viscous-delay time T_{vis} , the energy transfer efficiency ϵ , and the two parameters of R_0 and l_p to describe the photosphere. Moreover, there is an additional parameter of mag_0 to represent the contributions from stellar lights in host galaxies and/or from not apparent intrinsic AGN variability. Then, for the observed long-term variability of SDSS J1605, the well-known maximum likelihood method combined with Markov Chain Monte Carlo technique (Foreman-Mackey et al. 2013) can be applied to determine the best fitting results. Certainly, when the procedure above applied, there is only one limitation to the model parameters, leading to the determined tidal disruption radius $R_{TDE} \propto M_*^{-1/3} M_{BH}^{-2/3}$ larger than the event horizon $R_s = 2GM_{BH}/c^2$ of central BH.

Before proceeding further, there is one point we should note. The circularizations in TDEs as more recently discussed in Zanazzi & Ogilvie (2020); Lynch & Ogilvie (2021) are not considered in this Letter. Due to probably different fallback timescales for the circularizations and the accretion processes, two bright phases could be expected in light curves. However, as the shown CSS light curve of SDSS J1605, there are no clues on two bright phases. Therefore, we mainly consider the simple case that the fallback timescales of the circularizations are significantly smaller than the viscous timescales of the accretion processes, leading the fallback materials to circularize into a disk as soon as possible.

For SDSS J1605, the TDE model determined best-fitting results and the corresponding confidence bands by uncertainties of the TDE model parameters are shown in the left panel of Fig. 1 to the CSS V-band light curve. And right panels of Fig. 1 show the MCMC determined two-dimensional posterior distributions of the model parameters. The determined model parameters with $\gamma = 4/3$ are as follows: $\log(M_{BH,6}) \sim 2.16 \pm 0.07$, $\log(M_*/M_\odot) \sim 0.45 \pm 0.03$, $\log(\beta) \sim 0.20 \pm 0.04$, $\log(T_{vis}) \sim -0.91 \pm 0.14$, $\log(\epsilon) \sim -0.81 \pm 0.14$, $\log(R_0) \sim 0.52 \pm 0.19$, $\log(l_p) \sim 0.27 \pm 0.09$ and $\log(mag_0) = 1.2668 \pm 0.0004$. The TDE-model expected best descriptions to the light curve provide clues to support a potential TDE in the BLAGN SDSS J1605.

The TDE model determined BH mass is about $144_{-21} + 26 \times 10^6 M_\odot$ in SDSS J1605, certainly smaller than the corresponding Hills limit value $420 \times 10^6 M_\odot$ through the Equation (6) in Yao et al. (2023) after considering the larger stellar mass of the disrupted star in SDSS J1605, indicating the determined BH mass can be reasonably accepted in SDSS J1605. Meanwhile, as discussed in Yao et al. (2023) that TDE rate drops significantly with BH masses higher than $10^{7.5} M_\odot$, however massive stars being disrupted can lead to detectable TDEs with larger central BH masses.

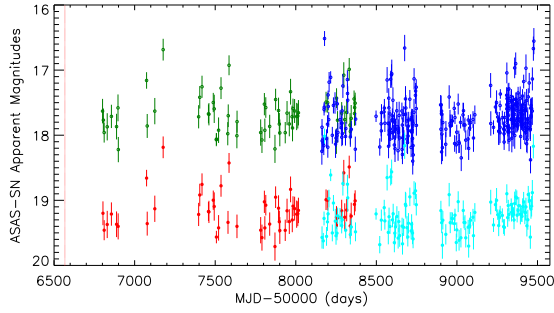


Figure 2. ASAS-SN light curves of SDSS J1605. Open circles plus error bars in dark green and in blue show the V-band and g-band data points. The vertical dotted red line marks the position for the ending time of the CSS light curve shown in Fig. 1. Solid circles plus error bars in red and in cyan show the corresponding 5days binned light curves (plus 1.5mag).

Moreover, besides the CSS light curve, the 7years-long V/g-band light curves can be collected from the ASAS-SN with MJD from about 6800 to 9500 for SDSS J1605, and also the 5days binned light curves shown in Fig. 2. There are not apparent trend variability in the ASAS-SN light curves, due to the linear function determined trend variability amplitudes about 0.07mag and 0.09mag in the V/g-band light curves, indicating that the bright flare around MJD~ 3000 – 5000 unique enough is not related to intrinsic AGN activity. Furthermore, similar as done in Hinkle et al. (2023b), the damped random walk process (Kelly et al. 2009; Kozłowski et al. 2010) is applied to describe the 5days binned ASAS-SN g-band light curve with determined variability timescale about 4.5days in rest frame through the public JAVELIN code (Zu et al. 2013), leading to the expected BH mass smaller than $10^{6.2}M_{\odot}$ through the results shown in Figure 8 in Hinkle et al. (2023b), which is very smaller than the TDE model determined BH mass and also very smaller than the virial BH mass discussed in section 3, indicating few effects of intrinsic AGN variability.

3 PROPERTIES OF EMISSION LINES IN SDSS J1605

SDSS spectrum of SDSS J1605 (plate-mjd-fiberid=2524-54568-0105) is shown in left panel of Fig. 3 with apparently broad $H\beta$ emission line with marked clear double-peaked features and also apparent broad UV Mg II emission line. Meanwhile, the composite spectrum of SDSS quasars (Vanden Berk et al. 2001) is also shown, to confirm the quasar-like spectroscopic features of SDSS J1605.

Similar as what have done in Zhang (2021b), multiple Gaussian functions are applied to describe the narrow emission lines around $H\beta$ with rest wavelength from 4700 to 5150Å, one extended and one narrow Gaussian components for the extended and core components of narrow $H\beta$ and [O III] doublet. And the elliptical accretion disk model discussed in Eracleous et al. (1995) is applied to describe the double-peaked broad $H\beta$, similar as what we have recently done in Zhang (2022d). Through the Levenberg-Marquardt least-squares minimization technique (the known MPFIT package), the best descriptions are shown in the top right panel of Fig. 3, with $\chi^2/dof \sim 1.01$ (χ^2 and dof as summed squared residuals and degree of freedom). The measured line parameters of the narrow lines and the disk model parameters of the double-peaked broad $H\beta$ are listed in Table 1. Meanwhile, the spectroscopic features of the broad UV Mg II emission line is shown in the bottom right panel of Fig. 3.

Based on the emission line properties, among the reported TDEs

candidates, SDSS J1605 has unique spectroscopic properties. First, among the reported TDEs candidates, only quite weak narrow forbidden emission lines can be detected in NUV and optical band. Even in the TDEs candidates of SDSS J0159 (a changing-look QSO) (Merloni et al. 2015; LaMassa et al. 2015) and PS16DTM (Blanchard et al. 2017) in the narrow line Seyfert I galaxy SDSS J015804.75-005221.8, there are apparent [O III] emission lines, however, the flux ratios O3HB of [O III] to narrow $H\beta$ are only 2.7 and 3.2. Similar lower O3HBs can be found in the other TDEs candidates, such as in XJ1500+0154 (Lin et al. 2017) with O3HB about 1.6. However, SDSS J1605 has the strongest narrow emission lines of [O III] doublet, with O3HB larger than 7, indicating strong and reliable central intrinsic AGN activity in SDSS J1605 through the applications of BPT diagram (Kewley et al. 2019; Kauffmann et al. 2003). Second, not only broad Balmer emission lines but also broad prominent He emission lines can be expected as spectroscopic properties of TDEs candidates, such as the cases in PS1-10jh (Gezari et al. 2012), AT2018hyz (Short et al. 2020), F01004-2237 (Thorpe et al. 2019), etc. However, SDSS J1605 have no apparent optical He II emission lines. Third, there are no reports on UV broad Mg II emission lines as spectroscopic properties of TDEs candidates. However, SDSS J1605 has apparent broad Mg II emission lines. Fourth, at the late times of TDEs, the double-peaked broad Balmer and He emission lines tightly related to TDEs debris are becoming quite weak, such as the cases in SDSS J0159 (Merloni et al. 2015), ASASSN-14li (Holoien et al. 2016), PTF09djl (Liu et al. 2017) etc. However, SDSS J1605, its spectrum observed at MJD=54568 marked by vertical solid red line in Fig. 1, has the broad Balmer emission lines being strong enough at late times of the expected TDE. Through the spectroscopic features of strong forbidden emission lines, strong broad Balmer emission lines at late times of TDE and strong UV broad Mg II emission lines, SDSS J1605 could be a normal BLAGN as the host galaxy of an expected central TDE, not similar as the host galaxy of any one of the reported optical TDEs.

If the broad $H\beta$ in SDSS J1605 was totally related to central TDE debris, the sizes of broad $H\beta$ emission regions could be similar as the geometric sizes of the TDE debris. Based on the commonly and well discussed accreting debris in Guillochon & Ramirez-Ruiz (2013), the TDE debris in SDSS J1605 at MJD=54568 have outer distance about $R_{out} \propto M_{BH}^{1/3, 2/3} \sim 22$ light – days $\sim 2200R_s$ and have inner distance about the $R_{in} \sim R_{TDE} \sim 2R_s$. Meanwhile, based on the elliptical accretion disk model to describe the double-peaked broad $H\beta$, the model determined inner and outer boundaries in units of R_s of the expected disk-like BLRs are about 63 and 530, the other five model parameters of the inclination angle i , the line emissivity slope q for the broad line emissions, the local broadening velocity σ_L , the eccentricity e and orientation angle ϕ_0 for the disk-like BLRs are listed in Table 1. The accretion disk model determined inner and outer boundaries for the disk-like structure are not beyond TDE model determined R_{out} , indicating double-peaked features of broad $H\beta$ cannot provide clues to be against the potential central TDE in SDSS J1605.

Meanwhile, through the improved R-L empirical relation for sizes of AGN BLRs in Bentz et al. (2013), the continuum luminosity ($\sim 3.23 \times 10^{44}$ erg/s) expected BLRs size is about 67light-days in SDSS J1605, three times larger than the outer distance of TDE debris. Then, combining with broad $H\beta$ with line width (second moment) about 2660 ± 240 km/s, the expected virial BH mass is about $M_{BH} \sim 8.83 \times 10^8 M_{\odot}$ through the virialization formula discussed in Peterson et al. (2004); Rafiee & Hall (2011), similar as the virial BH mass about $9.3 - 10.9 \times 10^8 M_{\odot}$ in Shen et al. (2011) for SDSS J1605. Apparently, the virial BH mass is about 7times larger than the

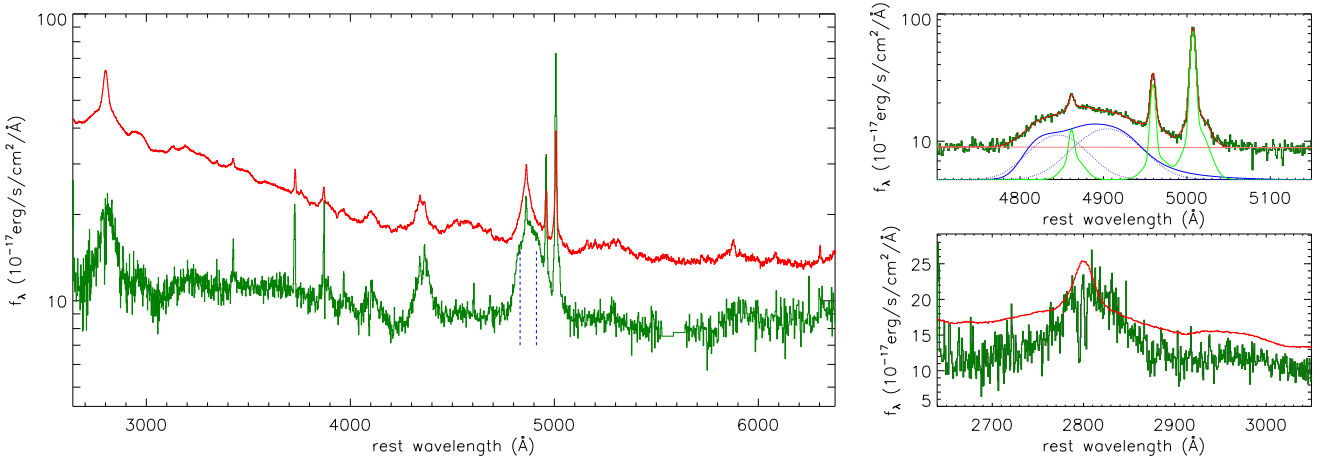


Figure 3. Left panel shows the SDSS spectrum (solid dark green line) of SDSS J1605 with plate-mjd-fiberid=2524-54568-0105. Solid red line shows the composite spectrum of SDSS quasars, vertical dashed blue lines mark positions of two peaks (or shoulders) of the broad H β . Top right panel shows the best descriptions (solid red line) to the emission lines around H β (solid dark green line). Solid pink line shows the determined power law component, solid blue line shows the determined broad H β (plus 5) by the accretion disk model, solid green lines show the determined both core (plus 5) and extended components (plus 5) of the narrow H β and the [O III] doublet, dotted blue lines show the determined broad Gaussian components (plus 5) in the broad H β described by broad Gaussian functions. Bottom right panel shows the emission line properties around Mg II. Solid dark green line shows the SDSS spectrum, solid red line shows the composite spectrum of SDSS quasars.

TDE model determined BH mass. Accepted TDE contributions leading to actual BLR sizes smaller than R-L relation estimated value, TDE model determined BH mass smaller than virial BH mass in SDSS J1605 can be reasonably explained. More accurate BH mass estimated by independent method in SDSS J1605 will provide clear clues to support or to be against the expected central TDE in SDSS J1605.

Furthermore, besides disk-like structure discussed above, double BLRs related to a binary black hole system (BBH system) (Begelman et al. 1980; Graham et al. 2015; Zhang 2023b,c) could also be applied to describe the double-peaked broad H β in SDSS J1605. If there was a BBH system in SDSS J1605, through the broad H β described by two broad Gaussian components shown as dotted blue lines in the top right panel of Fig. 3 with the corresponding parameters listed in Table 1, the central BH mass for the -1030 ± 130 km/s blue-shifted broad component should be about $2.5^{+0.5}_{-0.4}$ times of the central BH mass for the 2570 ± 142 km/s red-shifted broad component. However, simply accepted the Virialization assumptions, mass ratio of the central two BHs related to the blue-shifted and the red-shifted broad components in the broad H α can be estimated as $\frac{f_b^{0.5} \sigma_b^2}{f_r^{0.5} \sigma_r^2} \sim 0.64^{+0.36}_{-0.23}$ very smaller than the expected 2.5, with f_b , f_r , σ_b and σ_r as the emission line flux and the second moment of the blue-shifted and the red-shifted broad components in the broad H β . Thus the BBH system should be not favoured in SDSS J1605.

Before ending the section, one point is noted. Besides TDE model, several another scenarios can be applied to describe such optical flares in AGN (or called ambiguous nuclear transient events), such as the more recent discussions in Graham et al. (2017); Holoien et al. (2022); Hinkle et al. (2023b). Unfortunately, due to loss of multi-band variability properties and loss of time-dependent variability properties of spectroscopic features in SDSS J1605, it is hard to give further discussions on the other scenarios applied in SDSS J1605. In the near future, based on a small sample of such flares as the one in SDSS J1605 with double-peaked broad emission lines, further statistical clues could be provided.

In current stage, long-term variability properties of a sample of

BLAGN with double-peaked (or more complicated) broad emission lines are being carefully checked, after collected long-term light curves from both CSS and ZTF. We wish more TDE candidates can be discovered in BLAGN with double-peaked broad emission lines, and reported in the near future as soon as possible, after considering the basic point that BLAGN with double-peaked broad emission lines probably harboring potential TDEs candidates.

4 CONCLUSIONS

A potential TDE candidate is discovered in the double-peaked BLAGN SDSS J1605, especially through TDE expected variability pattern in the CSS light curve. Meanwhile, none apparent trend variability in the ASAS-SN light curves afterwards provide clues to support the CSS flare in SDSS J1605 is unique and different enough from variability of normal AGN. Furthermore, spectroscopic results can be applied to determine consistency between TDE determined geometric sizes of debris and sizes of emission regions of the double-peaked broad H β described by the accretion disk model, to support a central TDE in SDSS J1605. Moreover, the virial BH mass ~ 7 times higher than the TDE model determined BH mass can be accepted as one another independent evidence to support a central TDE in SDSS J1605. Although it is still a long way from totally confirmed conclusion on the double-peaked broad lines related to TDEs, the results in this Letter can provide clues to detect potential TDEs in double-peaked BLAGN.

ACKNOWLEDGEMENTS

Zhang gratefully acknowledge the anonymous referee for giving us constructive comments and suggestions to greatly improve our paper. Zhang gratefully thanks the kind financial support from GuangXi University and the kind financial support from NSFC-12173020 and NSFC-12373014. This Letter has made use of the data from the SDSS projects. The SDSS-III web site is <http://www.sdss3.org/>.

SDSS-III is managed by the Astrophysical Research Consortium for the Participating Institutions of the SDSS-III Collaboration. This letter has made use of the data from CSS funded by the National Aeronautics and Space Administration and by the U.S. National Science Foundation.

DATA AVAILABILITY

The data underlying this article will be shared on reasonable request to the corresponding author (xgzhang@gxu.edu.cn).

REFERENCES

- Anderson, M., Mooley, K., Hallinan, G., et al., 2020, *ApJ*, 903, 116
- Begelman, M. C., Blandford, R. D., Rees, M. J., 1980, *Natur*, 287, 307
- Bentz, M. C.; Denney, K. D.; Grier, C. J., et al., 2013, *ApJ*, 767, 149
- Blanchard, P. K.; Nicholl, M.; Berger, E., et al., 2017, *ApJ*, 843, 106
- Blagorodnova, N.; Gezari, S.; Hung, T.; et al., 2017, *ApJ*, 844, 46
- Chornock, R.; Berger, E.; Gezari, S.; Zauderer, B. A.; et al., 2014, *ApJ*, 780, 44
- Drake, A. J.; Djorgovski, S. G.; Mahabal, A., et al., 2009, *ApJ*, 696, 870
- Drake, A. J.; Djorgovski, S. G.; Mahabal, A., et al., 2011, *ApJ*, 735, 106
- Eracleous, M.; Livio, M.; Halpern, J. P.; Storchi-Bergmann, T., 1995, *ApJ*, 438, 610
- Foreman-Mackey, D.; Hogg, D. W.; Lang, D.; Goodman, J., 2013, *PASP*, 125, 306
- Gezari, S.; Martin, D. C.; Milliard, B., et al., 2006, *ApJL*, 653, 25
- Gezari, S.; Chornock, R.; Rest, A., et al., 2012, *Nature*, 485, 217
- Gezari S., 2021, *ARA&A*, 59, 21
- Graham, M. J.; Djorgovski, S. G.; Stern, D., et al., 2015, *Natur*, 518, 74
- Graham, M. J.; Djorgovski, S. G.; Drake, A. J.; et al., 2017, *MNRAS*, 470, 4112
- Gromadzki, M.; Hamanowicz, A.; Wyrzykowski, L.; et al., 2019, *A&A*, 622, 2
- Guillochon, J.; Ramirez-Ruiz, E., 2013, *ApJ*, 767, 25
- Guillochon, J.; Manukian, H.; Ramirez-Ruiz, E., 2014, *ApJ*, 783, 23
- Guillochon, J.; Nicholl, M.; Villar, A., et al., 2018, *ApJS*, 236, 6
- Hinkle, J. T.; Holoien, T. W. S.; Auchettl, K.; et al., 2021, *MNRAS*, 500, 1673
- Hinkle, J. T.; Tucker, M. A.; Shappee, B. J.; et al., 2023a, *MNRAS*, 519, 2035
- Hinkle, J. T.; Kochanek, C. S.; Shappee, B. J.; et al., *MNRAS*, 521, 3517
- Holoien, T. W.; Prieto, J. L.; Bersier, D.; et al., 2014, *MNRAS*, 445, 3263
- Holoien, T. W. S.; Kochanek, C. S.; Prieto, J. L.; et al., 2016, *MNRAS*, 455, 2918
- Holoien, T. W. S.; Huber, M. E.; Shappee, B. J.; et al., 2019, *ApJ*, 880, 120
- Holoien, T. W. S.; Neustadt, J. M. M.; Valley, P. J.; et al., 2022, *ApJ*, 933, 196
- Hung, T.; Foley, R. J.; Ramirez-Ruiz, E.; et al., 2020, *ApJ*, 903, 31
- Kauffmann, G.; Heckman, T. M.; Tremonti, C., et al., 2003, *MNRAS*, 346, 1055
- Kelly, B. C.; Bechtold, J.; Siemiginowska, A., 2009, *ApJ*, 698, 895
- Kewley, L. J.; Nicholls, D. C.; Sutherland, R. S., 2019, *ARA&A*, 57, 511
- Kozłowski, S.; Kochanek, C. S.; Udalski, A., et al., 2010, *ApJ*, 708, 927
- Kostrzewa-Rutkowska, Z.; Jonker, P. G.; Hodgkin, S. T.; et al., 2018, *MNRAS*, 481, 307
- LaMassa, S. M.; Cales, S.; Moran, E. C., et al., 2015, *ApJ*, 800, 144
- Lee, C. H.; Hung, T.; Matheson, T.; et al., 2020, *ApJL*, 892, 1
- Lin, D.; Guillochon, J.; Komossa, S., et al., 2017, *Natur Astron.*, 1, 33
- Liu, F. K.; Zhou, Z. Q.; Cao, R.; Ho, L. C.; Komossa, S., 2017, *MNRAS Letter*, 472, 99
- Loeb, A.; Ulmer, A., 1997, *ApJ*, 489, 573
- Lynch, E. M.; Ogilvie, G. I., 2021, *MNRAS*, 501, 5500
- Merloni, A.; Dwelly, T.; Salvato, A. G.; et al., 2015, *MNRAS*, 452, 69
- Mockler, B.; Guillochon, J.; Ramirez-Ruiz, E., 2019, *ApJ*, 872, 151
- Peterson, B. M.; Ferrarese, L.; Gilbert, K. M.; et al., 2004, *ApJ*, 613, 682
- Rafiee, A.; Hall, P. B., 2011, *ApJS*, 194, 42
- Rees, M. J., 1988, *Nature*, 333, 523
- Ryu, T.; Krolik, J.; Piran, T., 2020, *ApJ*, 904, 73
- Sazonov, S.; Gilfanov, M.; Medvedev, P.; et al., 2021, *MNRAS*, 508, 3820
- Shen, Y.; Richards, G. T.; Strauss, M. A.; et al., 2011, *ApJS*, 194, 45
- Short, P.; Nicholl, M.; Lawrence, A.; Gomez, S.; et al., 2020, *MNRAS*, 498, 4119
- Short, P.; Lawrence, A.; Nicholl, M.; et al., 2023, *MNRAS*, 525, 1568
- Stein, R.; van Velzen, S.; Kowalski, M.; et al., 2021, *Nature Astronomy*, 5, 510
- Stone, N. C.; Kesden, M.; Chang, R. M.; van Velzen, S.; *General Relativity and Gravitation*, 2019, 51, 30, arXiv:1801.10180
- Tadhunter, C.; Spence, R.; Rose, M.; Mullaney, J.; Crowther, P., 2017, *Nature Astronomy*, 1, 61
- Thorp, S.; Chadwick, E.; Sesana, A., 2019, *MNRAS*, 488, 4042
- Tout, C. A.; Pols, O.; Eggleton, P.; Han, Z., 1996, *MNRAS*, 281, 257
- van Velzen S.; Gezari S.; Cenko, S. B.; et al., 2019, *ApJ*, 872, 198
- Vanden Berk, D. E.; Richards, G. T.; Bauer, A.; et al., 2001, *AJ*, 122, 549
- van Velzen, S.; Farrar, Glennys R.; Gezari, S., et al., 2011, *ApJ*, 741, 73
- van Velzen, S.; Gezari, S.; Hammerstein, E.; et al., 2021, *ApJ*, 908, 4
- Wang, T.; Yan, L.; Dou, L., et al., 2018, *MNRAS*, 477, 2943
- Wyrzykowski, L.; Zielinski, M.; Kostrzewa-Rutkowska, Z.; et al., 2017, *MNRAS Letter*, 465, L114
- Yao, Y. H.; Ravi, V.; Gezari, S.; et al., 2023, *ApJL*, 955, 6
- Zanazzi, J. J.; Ogilvie, G. I., 2020, *MNRAS*, 499, 5562
- Zhang, X. G., 2021, *MNRAS Letter*, 500, 57
- Zhang, X. G., 2021b, *ApJ*, 909, 16, arXiv:2101.02465
- Zhang, X. G., 2022a, *ApJ*, 928, 182
- Zhang, X. G., 2022b, *MNRAS Letter*, 516, 66, Arxiv:2208.05253
- Zhang, X. G., 2022c, *MNRAS Letter*, 517, 71, Arxiv:2209.09037
- Zhang, X. G., 2022d, *ApJS*, 260, 31, ArXiv:2203.12810
- Zhang, X. G., 2023a, *MNRAS*, 526, 6015, Arxiv:2310.07095
- Zhang, X. G., 2023b, *MNRAS*, 526, 1588, Arxiv:2309.08078
- Zhang, X. G., 2023c, *MNRAS*, 525, 335, Arxiv:2307.09041
- Zhou, Z. Q.; Liu, F. K.; Komossa, S.; et al., 2021, *ApJ*, 907, 77
- Zu, Y.; Kochanek, C. S.; Kozłowski, S.; Udalski, A., 2013, *ApJ*, 765, 106